Electrohydrodynamic tip streaming and emission of charged drops from liquid cones

ROBERT T. COLLINS, JEREMY J. JONES, MICHAEL T. HARRIS AND OSMAN A. BASARAN*
School of Chemical Engineering, Purdue University, West Lafayette, Indiana 47907, USA
*e-mail: obasaran@ecn.purdue.edu

Published online: 2 December 2007; doi:10.1038/nphys807

When a liquid is subject to a sufficiently strong electric field, it can be induced to emit thin fluid jets from conical tip structures that form at its surface. Such behaviour has both fundamental and practical implications, from raindrops in thunderclouds to pendant drops in electrospray mass spectrometry. But the large difference in length scales between these microscopic/nanoscopic jets and the macroscopic drops and films from which they emerge has made it difficult to model the electrohydrodynamic (EHD) processes that govern such phenomena. Here, we report simulations and experiments that enable a comprehensive picture of the mechanisms of cone formation, jet emission and break-up that occur during EHD tip streaming from a liquid film of finite conductivity. Simulations show that EHD tip streaming does not occur if the liquid is perfectly conducting or perfectly insulating, and enable us to develop a scaling law to predict the size of the drops produced from jet break-up.

Four centuries ago, William Gilbert, Queen Elizabeth's personal physician, observed that electric fields can deform fluid interfaces[1]. In a series of papers with drops that are pendant from tubes, Zeleny[2] later showed that a sufficiently strong electric field can destabilize a fluid interface separating a drop from the surrounding air. In Zeleny's experiments and ones carried out more recently[3,4], an unstable interface takes on a conical shape, now referred to as a Taylor cone, and typically either a stream of drops or a fine jet that subsequently breaks up into drops is emitted from the cone's tip. Such electrohydrodynamic (EHD) tip streaming or cone-jetting phenomena, which are often referred to as electrospraying, occur widely in nature and technology. Well-known examples of cone-jetting include ejection of streams of small charged drops from pointed tips of raindrops in thunderclouds[5] and the immensely popular technique of electrospray mass spectrometry[6], which is used for assaying large biomolecules. Currently, electrosprays are finding application in an ever-growing number of areas including separations, powder synthesis, coatings and encapsulation for controlled release[7–10].

How does a cone-jet form and how does the thin jet that emanates from the cone's tip break up into small drops? Answering these questions theoretically has been elusive given the orders of magnitude disparity between the macroscopic free drop, pendant drop or film that is deformed into a conical shape by the electric field and the microscopic (nanoscopic) jet that issues from the cone. Previous theoretical studies have sidestepped these questions and have instead adopted the following two approaches. One involves the assumption that a steady cone-jet already exists and analyses the transition region between the Taylor cone and the jet[11–18]. In the case of steady cone-jetting from pendant drops, the primary goal of this approach is to relate the current carried by the jet and its radius to the flow rate in the tube. The other treats the jet independently of the cone-jet transition and focuses on the break-up of an infinite electrified jet into drops by temporal analysis[19,20].

Figure 1 shows EHD tip streaming from a liquid film predicted by simulation and observed in experiment (see Methods). In the simulations (see below), the liquid is treated as a Taylor–Melcher leaky dielectric or semi-insulator (see Methods). Figure 1b shows the Taylor cone, the tip streaming jet, the transition region between them, and the small drop that is about to pinch-off from the tip of the thin jet predicted by simulation. The inset of Fig. 1b shows a magnified view of the jet's tip, and also shows a micro-thread connecting the about-to-form drop to the jet. Figure 1c–f shows, in 2 ms intervals, the development of a tip streaming jet from a thin film of canola oil in an experiment that has been captured at 1,000 frames s^{-1} using a Kodak SR-Ultra digital camera. As shown in Fig. 1, the tip of the conical meniscus sharpens dramatically in the time interval separating Fig. 1c and d. A jet is clearly visible in Fig. 1e and well developed in Fig. 1f. Agreement between experiment and simulation is excellent[21]. Furthermore, the experiments show that the dynamics is axisymmetric, which justifies the use of that assumption in the algorithm described below.

EHD tip streaming is analysed here by solving the dimensionless, axisymmetric Navier–Stokes system for the velocity $\mathbf{v}$ and pressure p,

$$\frac{\partial \mathbf{v}}{\partial t} + \mathbf{v}\cdot\nabla\mathbf{v} = \mathrm{Oh}\left(-\nabla p + \nabla^2\mathbf{v}\right) \text{ in } \Omega_L \tag{1}$$

$$\nabla \cdot \mathbf{v} = 0 \text{ in } \Omega_L, \tag{2}$$

and Laplace's equation for the electric potential Φ, and hence electric field $\mathbf{E} = -\nabla\Phi$,

$$\nabla^2\Phi = 0 \text{ in } \Omega_L \text{ and } \Omega_G. \tag{3}$$

In the leaky-dielectric model[22,23], the bulk density of free charge is zero but the density of surface charge q along the L–G interface is

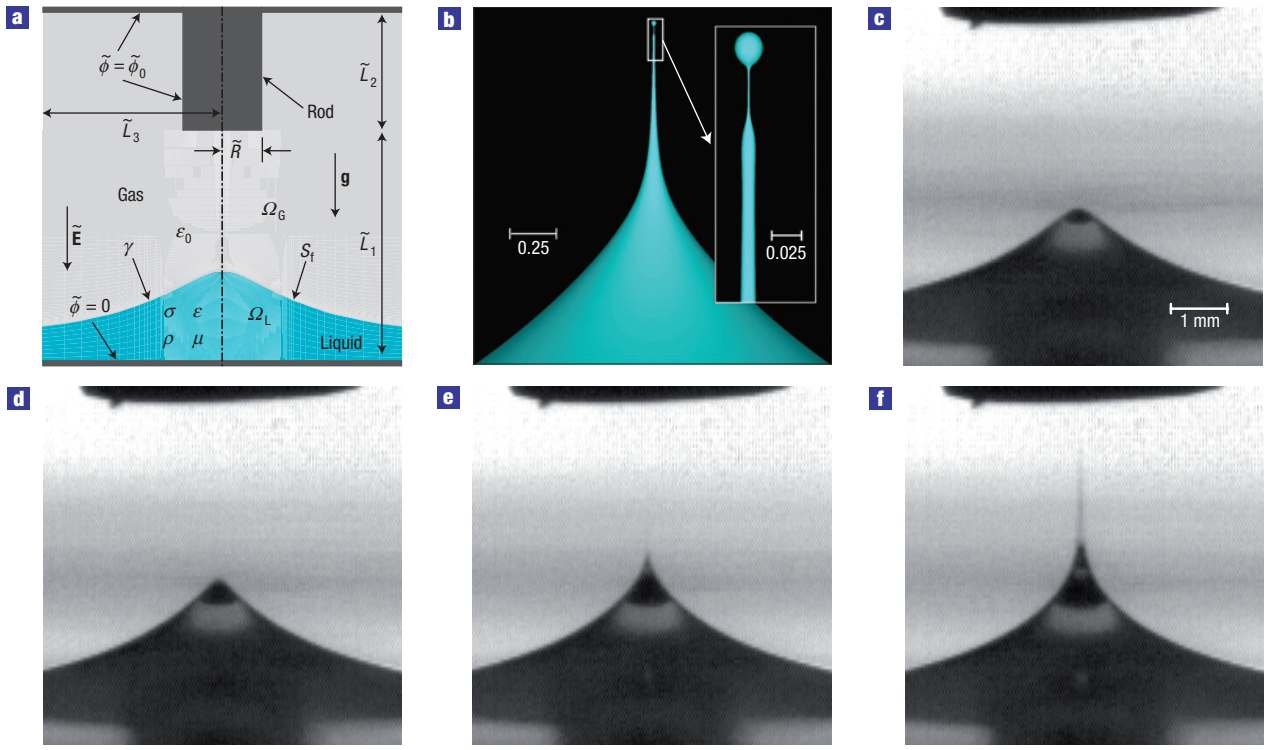

Figure 1 EHD tip streaming from a planar film. a, Definition sketch. **b**, Simulated tip streaming from a film of a leaky-dielectric liquid at the incipience of pinch-off: cone-jet (main image) and magnified view of the jet's tip (inset). Here, $\alpha = 0.75$, $\kappa = 7.5$, $\Gamma = 15$ and $\mathrm{Oh} = 0.1$. **c–f**, Experimental time sequence of tip streaming from a film of canola oil.

governed by a surface charge transport equation

$$\frac{\partial q}{\partial t} + \nabla_s \cdot (q\mathbf{v}) - \frac{1}{\mathrm{Pe}} \nabla_s^2 q = \frac{1}{\alpha} \mathbf{n} \cdot \mathbf{E}_L \text{ on } S_f. \qquad (4)$$

Here, $\mathbf{E}_L$ is the electric field evaluated along S_f on the liquid side, $\mathbf{n}$ is the unit vector normal to S_f and ∇_s is the surface gradient. The source term on the right side of equation (4) represents ohmic conduction of charge from the liquid to the free surface (see Methods). The electric field and the flow in the film are coupled through the traction condition along S_f,

$$-\mathrm{Oh}\, \mathbf{n} \cdot (-p + \nabla \mathbf{v} + (\nabla \mathbf{v})^{\mathrm{T}})$$
$$= -2\mathcal{H} + 2\Gamma \mathbf{n} \cdot \left[\left| \nabla \Phi \nabla \Phi - \frac{1}{2} \nabla \Phi \cdot \nabla \Phi \mathbf{I} \right| \right] \quad \text{on } S_f,$$

where $-2\mathcal{H}$ is twice the local mean curvature of the L–G interface and the notation $[|x|]$ denotes the jump in a quantity x, here the Maxwell stress, across the L–G interface. Also along the L–G interface, the tangential electric field is continuous but the electric displacement suffers a jump across S_f

$$q = \mathbf{n} \cdot (\kappa \nabla \Phi_L - \nabla \Phi_G) \text{ on } S_f,$$

where the subscripts L and G denote quantities evaluated on the liquid and the gas sides of S_f. The prohibition of mass transfer across S_f is guaranteed by the kinematic condition

$$\mathbf{n} \cdot (\mathbf{v} - \mathbf{v}_s) = 0 \text{ on } S_f,$$

where $\mathbf{v}_s$ is the velocity of points on S_f. The remaining boundary conditions are given in Methods.

Equations (1)–(4) are solved simultaneously as an initial-boundary-value problem using the finite-element method with elliptic mesh generation and adaptive, implicit time integration. Similar algorithms developed in our research group have been used to simulate dripping of taps, pinch-off singularities and flow focusing[24,25]. In contrast to the present approach, recent computational studies of break-up of electrified interfaces involved one or more simplifying assumptions. Most noteworthy among these are ref. 26 on the formation of drops of inviscid (limit of zero viscosity or $\mathrm{Oh} = 0$), perfectly conducting liquids and ref. 27 on the dynamics of sessile drops undergoing creeping flow (limit of infinite viscosity or $1/\mathrm{Oh} = 0$).

Direct numerical simulation of EHD tip streaming as an initial-boundary-value problem enables detailed examination for the first time of the early stages of the development of a cone-jet and the mechanism(s) responsible for its formation. In this regard, comparison of leaky-dielectric fluids with perfectly conducting fluids proves indispensable. Both perfectly conducting films and films of leaky-dielectric fluids of low to moderate σ and ϵ (Fig. 1a) deform under the application of the electric field, forming an axisymmetric hump coaxial with the upper cylindrical electrode. Above a critical Bond number Γ, such films destabilize, forming a dynamic Taylor cone in which the fluid is continuously accelerated in what is a nearly spherically symmetric flow. As the meniscus tip begins to sharpen, surface charge density q, fluid velocity $\mathbf{v}$ and tip curvature κ_{tip} grow rapidly. It is here that the similarity between conducting and leaky-dielectric films breaks down. Figure 2a shows the time evolution of κ_{tip} for both a conducting film and a leaky-dielectric film. For the conducting film, κ_{tip} tends to infinity in

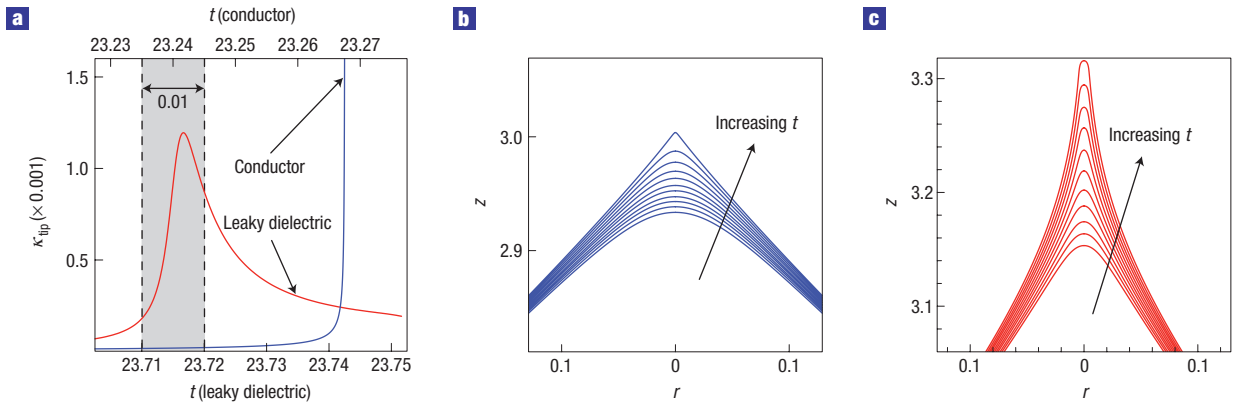

Figure 2 Curvatures and shapes of liquid films. a, Time evolution of the tip curvature κ_{tip} of a perfectly conducting film (blue) and a leaky-dielectric film (red). **b**,**c**, Meniscus profiles of the conducting film (**b**) and the leaky-dielectric film (**c**). Meniscus profiles are shown spanning the last 0.01 capillary times before the conic cusping singularity in **b** and for the grey shaded region of **a** in **c**. Here, Oh = 0.1 and $\Gamma = 15$ for both films and $\alpha = 0.75$ and $\kappa = 7.5$ for the leaky-dielectric film.

finite time, as do **v** and q at the meniscus tip. Indeed, the tip of the Taylor cone evolves in a spherically symmetric, self-similar manner, akin to what is observed with inviscid fluids and for which the term conic cusping singularity has been coined[28]. Figure 2b demonstrates the sharpening of the Taylor cone, showing meniscus profiles spanning the last 0.01 capillary times before the singularity. For the leaky-dielectric film, the time evolution of κ_{tip} exhibits a rapid growth (as with the conducting film), which then slows, undergoes a maximum, rapidly declines, and levels out (Fig. 2a). In this example, the span of the spike in κ_{tip} is 0.01 capillary times. Figure 2c demonstrates the change in the meniscus shape during this time span, corresponding to the greyed region in Fig. 2a. Here, the tip of the meniscus loses its conical geometry, revealing the emergence of a tip streaming jet. This sequence corresponds to the inception of tip streaming, which can be defined roughly as the time span between the first inflection point and the maximum of the κ_{tip} curve in Fig. 2a.

The conic cusping singularity can occur with perfectly conducting fluids because charge transport by ohmic conduction is instantaneous, that is, $\tilde{t}_e$ is always the shortest timescale in the system. As the meniscus tip sharpens owing to the spherically symmetric acceleration of the fluid, new charge is made available instantaneously so that the electrostatic pressure p_E, here $-(\Gamma/\mathrm{Oh})q^2$, continually balances the increasing capillary pressure p_C and preserves the driving force for the spherically symmetric flow. This is not the case with leaky-dielectric fluids. Here, as the tip of the conical meniscus sharpens, the fluid in the tip accelerates continuously, such that the local timescale for flow eventually becomes small with respect to the charge relaxation time. In Fig. 2, the dimensionless charge relaxation time $\alpha = 0.75$ and is hence nearly two orders of magnitude larger than the time span associated with the inception of tip streaming. In this spatiotemporal region, then, the dominant mode of charge transport switches from ohmic conduction of charge to S_f to charge convection along S_f. Charge cannot be brought to the meniscus tip fast enough for the electrostatic normal stress to balance the capillary pressure, which continues to increase owing to the inertia of the flow. Thus, the spherical symmetry of the flow is destroyed.

We are now in a position to illustrate the mechanism(s) responsible for the inception of EHD tip streaming with leaky-dielectric films. Figure 3a and b show the electric potential and axial velocity contours in the vicinity of the meniscus tip for a perfectly conducting fluid approaching the conic cusping singularity and a leaky-dielectric fluid at the inception of tip streaming, respectively. The conducting fluid is an equipotential, so that the internal electric field is identically zero, and the flow field, as discussed above, is spherically symmetric. A consequence of the lack of an internal electric field in the conducting fluid is that the tangential or shear component of the electric stress is zero along S_f. A very strong internal, axial electric field develops in the leaky-dielectric fluid in the vicinity of the meniscus tip at the inception of tip streaming. This is a consequence of the charge relaxation time vastly exceeding the flow timescale. Here, charge transport is dominated by charge convection and dilatation, so that surface charge is not distributed in a manner required to destroy the internal electric field. This combination of a high surface charge density and a strong axial electric field generates a strong electric shear stress ($\mathbf{n}\cdot\tau\cdot\mathbf{t} = q\,\mathbf{t}\cdot\mathbf{E}$) along S_f. Although a shear stress cannot deform an interface *per se*, it can act to accelerate the surrounding fluid through viscous transfer of axial momentum. For the case shown here, the size of the proto-jet, $O(10^{-2})$, is comparable to the dimensionless viscous length[29,30] $l_\mu = \mathrm{Oh}^2 = 0.01$, implying that the axial momentum is transferred efficiently to the entirety of the proto-jet, accelerating the proto-jet out of the Taylor cone.

Cross-sectional axial velocity profiles along the developing jet illustrate the significance of tangential stresses in the inception of tip streaming. In the case of conic cusping with a perfectly conducting fluid, the maximum axial velocity along a given cross-section occurs at the centre line $r = 0$ (Fig. 3c). This is a consequence of the spherical symmetry of the flow, which is driven entirely by normal electrostatic stresses. As the local timescale describing the flow at the tip of the cone becomes small with respect to the charge relaxation time, however, a dramatic reversal of the flow pattern is observed for the leaky-dielectric fluid, coinciding with the development of a large axial electric field near the tip of the cone. Significantly, as shown in Fig. 3d, the cross-sectional axial velocity in the developing jet is now maximum at the free surface and minimum at $r = 0$. This flow profile is strongly indicative of a shear stress-driven flow. The significance of electric stresses is further emphasized in Fig. 3e, which shows that the magnitude of the electric shear stress acting along S_f near the meniscus tip is comparable to that of the normal stresses acting there, that is, the electrocapillary pressure $p_E + p_C$ and viscous normal stress ($\mathbf{n}\cdot\tau\cdot\mathbf{n}$).

In the absence of electric shear stresses along S_f, we find that EHD tip streaming is not observed at all, as is shown in Fig. 3f. Computationally, this is accomplished by artificially

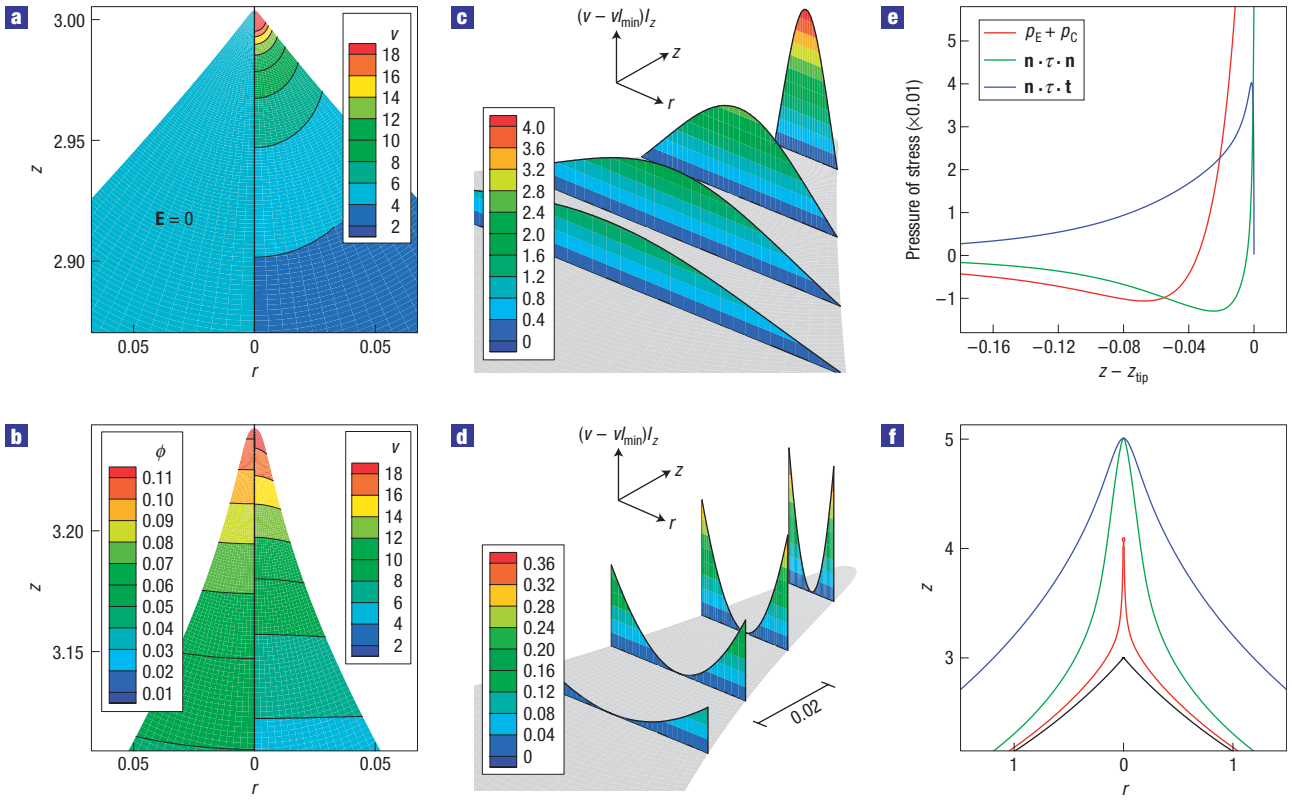

Figure 3 Flow and electric fields and stresses near the conic cusping singularity for a conducting film and at the inception of tip streaming for a leaky-dielectric film. a,**b**, Electric potential Φ and axial velocity v contours for a conducting film (**a**) and a leaky-dielectric film (**b**). **c**,**d**, The cross-sectional variation of the axial velocity for the conducting film (**c**) and the leaky-dielectric film (**d**). **e**, Variation of the electric shear stress $\mathbf{n}\cdot\tau\cdot\mathbf{t}$, the electrocapillary pressure $p_E + p_C$ and viscous normal stress $\mathbf{n}\cdot\tau\cdot\mathbf{n}$ from the tip of the meniscus for the leaky-dielectric film. **f**, EHD tip streaming observed with a leaky-dielectric film (red) is not observed when the shear component of the Maxwell stress along S_f is artificially 'turned off' (green). Profiles are shown for a perfectly insulating film (blue) and a perfectly conducting film (black) for comparison. Here, $\mathrm{Oh} = 0.1$ and $\Gamma = 15$ for all films, $\kappa = 7.5$ for the dielectric films and $\alpha = 0.75$ for the leaky-dielectric film.

'turning off' the appropriate term in the traction condition. Here, a profile for a leaky-dielectric film without electric shear stress (green) is shown alongside profiles for a leaky-dielectric fluid with the electric shear stress retained (red), a perfectly conducting fluid approaching the conic cusping singularity (black) and a perfectly insulating dielectric fluid (blue). When electric shear stresses are turned off, the leaky-dielectric fluid deforms in a manner more like a perfect insulator than a leaky-dielectric or a conductor, producing a fluid protuberance of the order of the global length scale. These results, taken together, strongly suggest that the primary mechanism for the inception of a tip streaming jet from a conical meniscus is the development of large electric shear stresses when the local flow timescale becomes small relative to α, in accordance with pioneering flow visualization experiments[31] and theoretical analyses[11–18] of steady cone-jetting from pendant drops.

The charge relaxation time α of the liquid comprising the film plays a critical role in EHD tip streaming. As $\alpha \to \infty$, ohmic conduction of charge to the free surface of the film becomes too slow to influence its deformation, which is instead driven by electric normal stresses related to the polarization of the film—this is the dielectric limit for which film deformation is independent of α. In contrast, as $\alpha \to 0$, ohmic conduction is so fast relative to all other mechanisms of charge transport that the electric field in the film becomes vanishingly small—this is the conductor limit for which EHD tip streaming gives way to the conic cusping singularity observed with perfectly conducting films. EHD tip streaming is observed only for intermediate values of α, and in this range α determines to a large degree the size of the tip streaming jet, and, hence, the size of the drops formed therefrom.

Figure 4a shows how the size of the drops formed from EHD tip streaming jets, and by extension the size of the jets themselves, varies with α when the other system parameters are held constant. Here, r_{drop} is the radius of a sphere of volume equal to that of the drop formed at pinch-off. The insets show jet profiles at pinch-off for $\alpha = 2.37$ (blue), $\alpha = 0.237$ (green) and $\alpha = 0.0237$ (red), the last of which produces a drop whose radius is only ~0.5% of the global length scale, or 5 μm for a 1 mm film. At low α, while still in the tip streaming regime, the drop size is found to follow precisely a power-law relationship, with $r_{drop} \sim \alpha^{1/3}$. At higher α, the size of the drops/jets formed begins to deviate from this power law, with the α dependence becoming progressively weaker as the perfect insulator or dielectric limit is approached. Figure 4b shows the influence of α on the transition region that connects the conical meniscus to the developed jet. Profiles are shown for the transition region of tip streaming jets corresponding to the insets in Fig. 4a, along with a profile for a perfectly conducting film approaching the conic cusping singularity (black). These profiles show that the transition region observed with tip streaming of leaky-dielectric films shrinks dramatically as α is decreased to approach the shape of the conical meniscus observed with perfectly conducting films approaching the conic cusping singularity (see Methods).

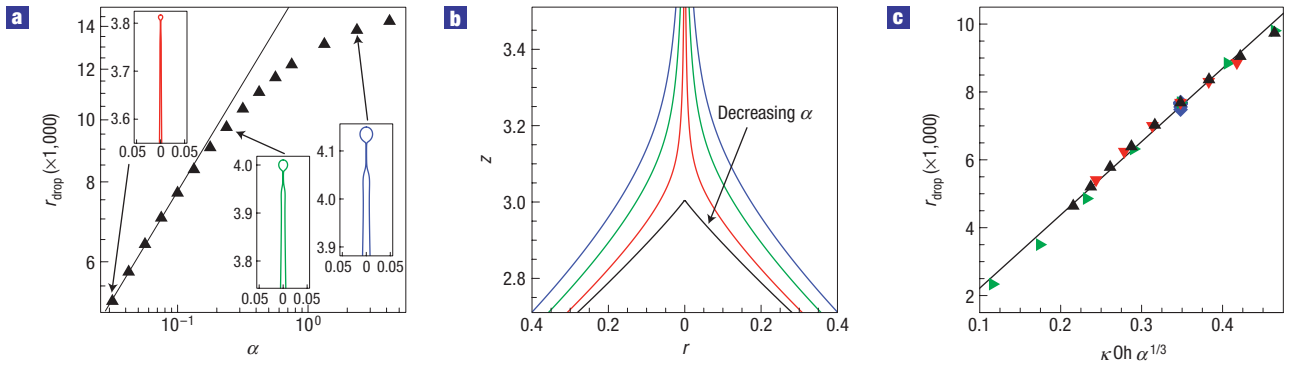

Figure 4 Scaling of drop size in EHD tip streaming. a, Radii r_{drop} of drops formed at pinch-off from tip streaming jets as a function of dimensionless electrical relaxation time α. The insets show jet profiles at the incipience of pinch-off for $\alpha = 2.37$ (blue), $\alpha = 0.237$ (green) and $\alpha = 0.0237$ (red). The size of the drops formed asymptotically approaches the power law $r_{drop} \sim \alpha^{1/3}$ (solid black line) as α decreases. Here and in **b**, $\Gamma = 15$, Oh $= 0.1$ and $\kappa = 7.5$. **b**, As α decreases, the size of the transition region between the conical meniscus and the developed jet decreases, and the conical meniscus approaches that which results with a perfectly conducting film of the same Γ and Oh. Meniscus profiles are shown for $\alpha = 2.37$ (blue), $\alpha = 0.237$ (green), $\alpha = 0.0237$ (red) and the perfect conductor (the black cone). Here, $\kappa = 7.5$, Oh $= 0.1$ and $\Gamma = 15$. **c**, Simulations show that the size of the drops formed varies as $r_{drop} \sim \kappa$ Oh $\alpha^{1/3}$ (solid black line). The coloured symbols indicate results from simulations for which one of the quantities κ (green), Oh (red), α (black) and Γ (blue) is varied while the others are held fixed.

A large number of simulations carried out in the regime where drop radius varies as $\alpha^{1/3}$ reveal that $r_{drop} \sim \kappa\,\mathrm{Oh}\,\alpha^{1/3}$ (Fig. 4c). How does this result compare with estimates of drop size from previous studies of steady cone-jetting? The two popular 'scaling laws' for the size of the drops formed from steady cone-jets are those of Fernández de la Mora and Loscertales[13] and Gañán-Calvo[14], which have been experimentally tested[15,32]. The first law states that the dimensional drop radius $\tilde{r}_D \sim (\tilde{Q}\tilde{t}_e)^{1/3}$, where $\tilde{Q}$ is the inlet fluid feed rate in the capillary tube for a steady cone-jet system. The second law proposes that the dimensional drop radius $\tilde{r}_G \sim \tilde{Q}^{1/2}(\tilde{t}_e\rho/\gamma)^{1/6}$. As EHD tip streaming is a local phenomenon for which there is no imposed flow rate, $\tilde{Q}$ should only depend on the properties of the liquid. If viscous effects are unimportant, $\tilde{Q} = \gamma\epsilon/\rho\sigma = \tilde{t}_e(\gamma/\rho)$ (refs 9,14). Then, both scaling laws predict that $\tilde{r}_D \sim \tilde{r}_G \sim (\gamma/\rho)^{1/3}\tilde{t}_e^{2/3}$. When made dimensionless, these scaling laws become $r_D \sim r_G \sim \alpha^{2/3}$. If, however, viscous effects are important, an alternative expression for the characteristic flow rate is $\tilde{Q} = \tilde{l}_\mu^3/\tilde{t}_\mu$, where $\tilde{l}_\mu$ is the viscous length and $\tilde{t}_\mu$ is the viscous time[29,30]. Then, the dimensional drop radius should scale as $\tilde{r}_\mu \sim \tilde{l}_\mu(\tilde{t}_e/\tilde{t}_\mu)^{1/3} = (\mu^3\epsilon/\rho^2\gamma\sigma)^{1/3}$. In dimensionless form, this expression becomes $r_\mu \sim \mathrm{Oh}\,\alpha^{1/3}$, which is identical in form to the expression reported above that resulted from fitting the simulation results. Plainly, comparison of the two estimates for the drop size, r_D or r_G and r_μ, reveals that there should be a transition between the two regimes and that viscous effects are unimportant when $\alpha^{1/3}/\mathrm{Oh} \gg 1$. This criterion accords with studies of steady cone-jetting where previous investigators have stated that for viscous effects to be negligible $\Pi \equiv \alpha^{1/3}/\mathrm{Oh} \gg 1$ (ref. 13).

According to the foregoing results, the new algorithm developed to analyse the transient development of EHD tip streaming has unparalleled accuracy in that it is able to resolve in a single simulation length scales that differ by four orders of magnitude and make predictions that accord well with experimental measurements. Having demonstrated the capabilities of the new approach in the present setting, we can now turn our attention to analysis of diverse situations involving cone-jets that also have defied adequate theoretical understanding so far. Exciting avenues of future study include steady cone-jetting from pendant drops[32], transient cone-jetting from free, for example, levitated, drops[5,33], Taylor cone formation in two-fluid jets[34] and electroflow focusing where both flow and electric field are used in tandem to produce very fine jets[35]. A crucial issue in all of these situations is the sizes of the drops formed from the break-up of the jets. Gañán-Calvo[18] has shown in a theoretical study of steady cone-jets the existence of six different regimes where distinct scaling laws govern the sizes of the drops formed. Some of these laws, two of which predict r_D and r_G reported above, are independent of viscosity μ. Two laws given in ref. 18 involve viscosity but predict that drop size is proportional to μ^a, where $a \neq 1$. The new scaling law proposed here predicts that drop size varies linearly with μ. Thus, future simulations should be used in concert with experiments and theory to build on the pioneering work of Gañán-Calvo[18] to improve our understanding of various scaling laws and the relationships among them.

METHODS

SYSTEM

The system (Fig. 1a) consists of a liquid film, which in the absence of electric field has constant thickness $\tilde{L}_0$, that sits on a horizontal metallic plate and is overlaid by an insulating gas, which is in turn covered by a second metallic plate, forming a parallel-plate capacitor. Protruding from the upper plate to a distance $\tilde{L}_1$ from the lower plate is a metallic cylindrical rod of radius $\tilde{R}$ and length $\tilde{L}_2$ whose axis is perpendicular to the two plates and parallel to the gravitational acceleration **g**. The liquid film (Ω_L) is a slightly conducting, incompressible newtonian fluid with density ρ, viscosity μ, permittivity ϵ and conductivity σ, whereas the gas (Ω_G) is a perfectly insulating and dynamically inactive fluid with permittivity ϵ_0. The surface tension γ of the liquid–gas (L–G) interface (S_f) and the physical properties of the two phases are taken to be constant and spatially uniform. At time $\tilde{t} = 0$, a potential difference $\tilde{\Phi}_0$ is imposed impulsively between the two electrodes, generating electric stresses that deform the initially flat, quiescent liquid film. Others have also used liquid films to study experimentally EHD instabilities[36,37].

DIMENSIONLESS GROUPS

The problem is cast into a dimensionless form using the capillary timescale $\tilde{t}_c \equiv \sqrt{\rho\tilde{L}_0^3/\gamma}$, length scale $\tilde{L}_0$, stress scale $\mu/\tilde{t}_c$, electric potential scale $\tilde{\Phi}_0$ and surface charge density scale $\epsilon_0\tilde{\Phi}_0/\tilde{L}_0$. Here, the variables without a tilde are the dimensionless counterparts of those with a tilde. Aside from the four dimensionless geometric parameters $L_1 \equiv \tilde{L}_1/\tilde{L}_0$, $L_2 \equiv \tilde{L}_2/\tilde{L}_0$, $L_3 \equiv \tilde{L}_3/\tilde{L}_0$ (the location of the asymptotic boundary) and $R \equiv \tilde{R}/\tilde{L}_0$, six other dimensionless groups arise: (1) Ohnesorge number $\mathrm{Oh} \equiv \mu/\sqrt{\rho\gamma\tilde{L}_0}$, (2) gravitational Bond number $G \equiv \rho g\tilde{L}_0^2/\gamma$, (3) electric Bond number

$\Gamma \equiv \epsilon_0 \tilde{\Phi}_0^2/2\gamma\tilde{L}_0$, (4) permittivity ratio $\kappa \equiv \epsilon/\epsilon_0$, (5) dimensionless charge relaxation time $\alpha \equiv \tilde{t}_e/\tilde{t}_c$, where $\tilde{t}_e \equiv \epsilon/\sigma$ is the charge relaxation time and (6) Peclet number $\mathrm{Pe} \equiv (\tilde{L}_0^2/D)/\tilde{t}_c$, where D is the surface diffusion coefficient and $\tilde{L}_0^2/D$ is the timescale for surface charge diffusion along S_f. For the simulation results presented, $L_1 = 6$, $L_2 = 4$, $L_3 = 10$, $R = 1$ and $G = 0$.

PECLET NUMBER

Surface charge diffusion is typically insignificant relative to other modes of charge transport but is included for completeness. All results discussed herein use $\mathrm{Pe} = 10^3$, as any increase in Pe above $O(10^3)$ has been shown to have no effect on the dynamics.

BOUNDARY CONDITIONS

Dirichlet conditions on Φ are imposed along the electrodes and the no-slip/no-penetration condition is imposed on $\mathbf{v}$ along the lower electrode. Symmetry conditions on the flow, electric field and interface shape are set along the centre line. Finally, asymptotic boundary conditions are imposed on these variables along the cylindrical boundary located at L_3.

DEPENDENCE ON ELECTRIC BOND NUMBER

Simulations show that tip streaming is not observed below a critical value of the electric bond number Γ_{Crit}. For $\Gamma < \Gamma_{\mathrm{Crit}}$, the film forms a hump and undergoes a steady, recirculating flow driven by electrically induced shear stress at the L–G interface. For $\Gamma > \Gamma_{\mathrm{Crit}}$, the drop/jet size varies negligibly with Γ and the geometric parameters of the system.

Received 25 July 2007; accepted 2 November 2007; published 2 December 2007.

References

1. Gilbert, W. *De Magnete* (Dover, 1958) (First published in Latin in 1600 and translated by P. F. Mottelay in 1893).
2. Zeleny, J. Instability of electrified liquid surfaces. *Phys. Rev.* **10**, 1–6 (1917).
3. Taylor, G. I. Disintegration of water drops in an electric field. *Proc. R. Soc. Lond. A* **280**, 383–397 (1964).
4. Cloupeau, M. & Prunet-Foch, B. Electrostatic spraying of liquids in cone-jet mode. *J. Electrostat.* **22**, 135–159 (1989).
5. Achtzehn, T., Müller, R. & Leisner, T. The Coulombic instability of charged microdroplets: Dynamics and scaling. *Eur. Phys. J. D* **34**, 311–313 (2005).
6. Fenn, J., Mann, M., Meng, C., Wong, S. & Whitehouse, C. Electrospray ionization for mass-spectrometry of large biomolecules. *Science* **246**, 64–71 (1989).
7. Ptasinski, K. J. & Kerkhof, P. J. A. M. Electric-field driven separations—phenomena and applications. *Sep. Sci. Technol.* **27**, 995–1021 (1992).
8. Harris, M. T., Scott, T. C. & Byers, C. H. The synthesis of metal hydrous oxide particle by multiphase electrodispersion. *Mater. Sci. Eng. A* **168**, 125–129 (1993).
9. Barrero, A. & Loscertales, I. Micro- and nanoparticles via capillary flows. *Annu. Rev. Fluid Mech.* **39**, 89–106 (2007).
10. Fernández de la Mora, J. The fluid dynamics of Taylor cones. *Annu. Rev. Fluid Mech.* **39**, 217–243 (2007).
11. Mestel, A. J. The electrohydrodynamic cone-jet at high Reynolds number. *J. Aerosol Sci.* **25**, 1037–1047 (1994).
12. Shtern, V. & Barrero, A. Striking features of fluid-flows in Taylor cones related to electrosprays. *J. Aerosol Sci.* **25**, 1049–1063 (1994).
13. Fernández de la Mora, J. F. & Loscertales, I. The current emitted by highly conducting Taylor cones. *J. Fluid Mech.* **260**, 155–184 (1994).
14. Gañán-Calvo, A. M. Cone-jet analytical extension of Taylor's electrostatic solution and the asymptotic universal scaling laws in electrospraying. *Phys. Rev. Lett.* **79**, 217–220 (1997).
15. Gañán-Calvo, A. M., Dávila, J. & Barrero, A. Current and droplet size in the electrospraying of liquids. Scaling laws. *J. Aerosol Sci.* **28**, 249–275 (1997).
16. Cherney, L. T. Electrohydrodynamics of electrified liquid menisci and emitted jets. *J. Aerosol Sci.* **30**, 851–862 (1999).
17. Higuera, F. Flow rate and electric current emitted by a Taylor cone. *J. Fluid Mech.* **484**, 303–327 (2003).
18. Gañán-Calvo, A. M. On the general scaling theory for electrospraying. *J. Fluid Mech.* **507**, 203–212 (2004).
19. López-Herrera, J. M., Gañán-Calvo, A. M. & Perez-Saborid, M. One-dimensional simulation of the breakup of capillary jets of conducting liquids. Applications to E.H.D. spraying. *J. Aerosol Sci.* **30**, 895–912 (1999).
20. López-Herrera, J. M. & Gañán-Calvo, A. M. A note on charged capillary jet breakup of conducting liquids: Experimental validation of a viscous one-dimensional model. *J. Fluid Mech.* **501**, 303–326 (2004).
21. Collins, R. T. *Deformation and Breakup of Liquid Films, Jets and Drops in Electric Fields*. Thesis, Purdue Univ. (2007).
22. Melcher, J. R. & Taylor, G. I. Electrohydrodynamics: a review of the role of interfacial shear stresses. *Annu. Rev. Fluid Mech.* **1**, 111–146 (1969).
23. Saville, D. A. Electrohydrodynamics: The Taylor–Melcher leaky dielectric model. *Annu. Rev. Fluid Mech.* **29**, 27–64 (1997).
24. Chen, A. U., Notz, P. K. & Basaran, O. A. Computational and experimental analysis of pinch-off and scaling. *Phys. Rev. Lett.* **88**, 4501 (2002).
25. Suryo, R. & Basaran, O. A. Tip streaming from a liquid drop forming from a tube in a co-flowing outer fluid. *Phys. Fluids* **18**, 082102 (2006).
26. Notz, P. K. & Basaran, O. A. Dynamics of drop formation in an electric field. *J. Colloid Interface Sci.* **213**, 218–237 (1999).
27. Reznik, S. N., Yarin, A. L., Theron, A. & Zussman, E. Transient and steady shapes of droplets attached to a surface in a strong electric field. *J. Fluid Mech.* **516**, 349–377 (2004).
28. Zubarev, N. M. Formation of conic cusps at the surface of liquid metal in electric field. *JETP Lett.* **73**, 544–548 (2001).
29. Eggers, J. Universal pinching of 3D axisymmetric free-surface flow. *Phys. Rev. Lett.* **71**, 3458–3460 (1993).
30. Lister, J. R. & Stone, H. A. Capillary breakup of a viscous thread surrounded by another viscous fluid. *Phys. Fluids* **10**, 2758–2764 (1998).
31. Hayati, I., Bailey, A. I. & Tadros, T. F. Mechanism of stable jet formation in electrohydrodynamic atomization. *Nature* **319**, 41–43 (1986).
32. Gamero-Castaño, M. & Hruby, V. Electric measurements of charged sprays emitted by cone-jets. *J. Fluid Mech.* **459**, 245–276 (2002).
33. Grimm, R. & Beauchamp, J. Dynamics of field-induced droplet ionization: Time-resolved studies of distortion, jetting, and progeny formation from charged and neutral methanol droplets exposed to strong electric fields. *J. Phys. Chem. B* **109**, 8244–8250 (2005).
34. Marín, A., Loscertales, I., Marquez, M. & Barrero, A. Simple and double emulsions via coaxial jet electrosprays. *Phys. Rev. Lett.* **98**, 014502 (2007).
35. Gañán-Calvo, A. M. Electro-flow focusing: The high-conductivity low-viscosity limit. *Phys. Rev. Lett.* **98**, 134503 (2007).
36. Taylor, G. I. & McEwan, A. D. The stability of a horizontal fluid interface in a vertical electric field. *J. Fluid Mech.* **22**, 1–15 (1965).
37. Oddershede, L. & Nagel, S. R. Singularity during the onset of an electrohydrodynamic spout. *Phys. Rev. Lett.* **85**, 1234–1237 (2000).

Acknowledgements

This work was supported by the Shreve Trust Fund at Purdue University and the BES Program of US DOE.
Correspondence and requests for materials should be addressed to O.A.B.

Author contributions

R.T.C.: theoretical and numerical work, article writing; J.J.J.: experimental work; M.T.H.: project planning; O.A.B.: theoretical work, project planning, article writing.